British Journal of Cancer www.nature.com/bjc

ARTICLE OPEN

Check for updates

Cellular and Molecular Biology

Integrative proteo-genomic profiling uncovers key biomarkers of lapatinib resistance in HER2-positive breast cancer

J. Steggall[1], V. Rajeeve[2], N. Al-Subaie[3], A. Naeem[1], A. Ikram[1], A. Naeem[4,5] and A. Hayat[1]✉

INTRODUCTION: Drug resistance is a major obstacle to the long-term effectiveness of cancer therapies. Approximately 70% of breast cancer patients relapse after 5 years of treatment, and the lack of biomarkers associated with drug resistance translates to poor prognosis in the clinic. Previous research has utilised omics approaches to uncover biomarkers driving drug resistance, with a strong emphasis on genetic mutations.

METHODS: Here, we identified a nine-marker signature associated with resistance to lapatinib in a HER2-positive breast cancer model using a target discovery approach by employing an integrative multi-omics strategy, combining ATAC-seq, RNA-seq and proteomics.

RESULTS: We found that seven markers in the drug resistance-signature had not been previously found to be implicated in HER2-positive breast cancer, some of which we further validated using an additional lung cancer model. We counterintuitively found that drug-resistant cells have restrictive chromatin accessibility with reduced gene expression associated with limited total proteome changes. However, upon closer look, we identified that the drug resistance-signature had increased chromatin accessibility near the transcriptional start sites of those seven markers and was highly differentially expressed across the three datasets. Our data show that despite the overall transcriptional and proteomic landscape showing limited changes, there are several markers that are highly expressed, which correlate with increased anchorage-independent and invasive phenotype in vitro in lapatinib-resistant cells compared to cancer cells.

CONCLUSIONS: Our results demonstrate that disease aggressiveness can be related to reduced chromatin and gene expression dynamics. We anticipate that the resistant signature identified here using an integrative target discovery approach can be applied to complex, more representative models and validated before they can be targeted by suitable therapeutic agents.

British Journal of Cancer; https://doi.org/10.1038/s41416-025-03174-3

INTRODUCTION

Breast cancer is the most commonly diagnosed cancer worldwide, with one in five cases exhibiting the overexpression of the Human Epidermal Growth Factor Receptor 2 (HER2). Despite significant advancements in treatment in recent years, more than 70% of patients relapse after 5 years, indicating the need to interrogate the mechanisms of acquired drug resistance [1]. Integrative multi-omics approaches are a powerful tool in aiding to elucidate the aberrant changes driving acquired drug resistance. Identifying novel biomarkers and understanding the molecular mechanisms contributing to acquired drug resistance are vital for tackling cancer dissemination and metastasis.

Lapatinib, a dual kinase inhibitor, targets HER2 and Epidermal Growth Factor Receptor (EGFR) domains, thereby preventing phosphorylation and subsequent signal transduction of the mitogen-activated protein kinase (MAPK) and phosphoinositide 3-kinase/Akt pathways, leading to cell death [2]. Lapatinib is frequently used in combination with other therapeutic agents for treating high-risk metastatic breast cancer patients, particularly in cases where they display resistance to trastuzumab, a first-line therapeutic agent for HER2-positive breast cancer [3, 4]. Despite initial efficacy, most patients inevitably develop resistance to lapatinib and, sadly, succumb to disease progression and mortality [5]. A major challenge remains in how we overcome this resistance. The selective pressure as a result of targeted therapies on HER2 leads to rapid evolution of acquired drug resistance mechanisms, reducing the efficacy of personalised medicine approaches, resulting in disease relapse [6].

A growing number of changes have been identified in the genome and the epigenome of breast cancer cell lines, with the upregulation of *SCIN* and *GIRK1* playing a key role in promoting proliferation and inhibiting apoptosis. Alongside this, the

[1]Department of Molecular and Biomedical Sciences, City St George's, University of London, London, UK. [2]Mass Spectrometry Facility, Barts Cancer Institute, Queen Mary University of London, John Vane Science Centre, London, UK. [3]Department of Mathematics and Statistics, Al-Khurmah University College, Taif University, Taif, Saudi Arabia. [4]Department of Basic Sciences, College of Science and Health Professions, King Saud bin Abdulaziz University for Health Sciences, Jeddah, Saudi Arabia. [5]King Abdullah International Medical Research Center, Jeddah, Saudi Arabia. ✉email: ahayat@sgul.ac.uk

Received: 9 January 2025 Revised: 23 July 2025 Accepted: 20 August 2025
Published online: 13 September 2025

downregulation of *EGR1* leads to the overexpression of multidrug resistance protein 1 *(MDR1)*, contributing to poor prognosis and therapeutic resistance [7–10]. However, despite these advancements in identifying several proteins associated with acquired drug resistance, the transcriptome and particularly the chromatin dynamics remain largely unexplored, informing our integrative approach to perform deep-sequencing analysis of high HER2 expressing cancer cells (SKBR3) and its lapatinib-resistant counterpart (SKBR3-L) using multi-omics. Chromatin accessibility is a key regulator of gene expression and alterations in the chromatin state can lead to significant changes in transcriptional activity, which are eventually translated into proteins, the effectors of cell function [11]. Nevertheless, DNA alterations and changes in RNA expression do not always translate into protein expression patterns that cause distinct biological changes in cell function at the level where targeted therapies work [12]. Therefore, using a combination of omics techniques that allow us to characterise a snapshot of the molecular landscape at several different layers of regulation is likely to define molecular changes critical for acquired drug resistance.

After we identified specific genomic regions and transcription factors (TFs) that play a crucial role in regulating gene expression using (assay of transposase-accessible chromatin using sequencing) ATAC-seq and RNA-seq. We conducted an unbiased global proteome analysis of the same cells to catalogue the intricate workings of lapatinib resistance at the protein level. By exploring the genome, transcriptome and proteome at each level, we developed a comprehensive understanding of drug resistance in these cells. This integrated approach helped uncover the underlying changes that may contribute to drug resistance. These findings could pave the way for further validation of biomarkers in additional models, which could lead to clinical validation. Ultimately, this could improve the efficacy of HER2-targeted therapies using a sequence of biomarker-guided therapies that result in a cure [13]. We unexpectedly discovered a significant decrease in chromatin accessibility, which aligned with changes in gene expression patterns in the drug-resistant cells. These changes were associated with limited alterations in the proteome. However, certain regions of the genome remained highly accessible at the chromatin level, near the promoter, which could be contributing to the aggressive nature of drug-resistant cells.

RESULTS

Lapatinib resistance evokes aggressive in vitro transformation

To explore the stochastic changes associated with acquired drug resistance, we obtained SKBR3 cells, which express high levels of HER2 protein with an established cell line model of acquired resistance to lapatinib, SKBR3-L cells (Fig. 1a) [6]. We first tested the robustness of the system by analysing the HER2 protein expression using immunofluorescence. HER2 protein expression was observed in both SKBR3 and SKBR3-L cells; however, levels were reduced in the SKBR3-L cell line (Fig. 1b; Supplementary Fig. 1A). We next sought to establish whether there were differences in the morphological profiles between the two cell types. Cells were embedded into a 3D matrix and phase-focus quantitative time-lapse imaging was performed over 15 h, allowing for a detailed examination of cell behaviour and morphology. Intriguingly, automated tracking revealed initial subtle decreases in perimeter in SKBR3-L cells, which then stabilised, in contrast to the more pronounced perimeter reduction in SKBR3 cells (Fig. 1c). Throughout the experiment, SKBR3-L cells exhibited consistently reduced sphericity, assuming more irregular shapes and protrusions indicative of invasive capabilities. Additionally, despite an overall reduction in size, SKBR3-L maintained a larger cellular area, suggesting not only structural but also potentially functional adaptations conducive to invasive growth and metastatic potential as cells attempt to colonise the remaining space. We carried out soft agar colony formation assays, a gold standard for assessing in vitro transformation, to test whether drug-resistant cells have higher transformational potential compared to cancer cells. SKBR3-L cells consistently formed enlarged structures in soft agar compared to SKBR3 cells across three different sizes, underscoring their highly transformed and drug-resistant nature (Fig. 1d, e).

Identification of a distinct reduction in transcriptomic profile in acquired drug resistance

To characterise how the genomic landscape differs between cancer cells and their lapatinib-resistant counterparts, we performed RNA-seq to determine gene expression patterns between the two cell types. The transcriptional programme of breast cancer cells and drug-acquired resistant cells differed significantly. Principal component analysis (PCA) separated the samples into two distinct clusters, confirming the difference between sensitive and resistant cell types (Fig. 2a). Notably, after the development of resistance, the cell line adopted a similar genetic profile, suggesting the emergence of a common adaptive response to therapy.

We assessed the differential gene expression between these two groups and discovered that 8.5% were highly expressed genes with log2fold > 1, p value < 0.05. Conversely, ~19% of the genes were downregulated with log2fold < −1, p value < 0.05 (Fig. 2b, c). We confirmed the differential upregulation of previously known genes in such as *SCIN, CALD1* and *MCAM*, which have been associated with aggressive, basal-like phenotype and in acquired drug resistance in cancer [14–16]. However, we found novel genes such as *MORN3* with an unknown function, and *WIPF1*, which is an important differentiation marker but is not known to be involved in acquired drug resistance, both of which could be important as potential therapeutic resistance targets. Intriguingly, we identified *EGR1* to be significantly downregulated, which is implicated in breast cancer resistance and an important epigenetic regulator in the methylation context, but whose function in HER2-positive breast cancer has yet to be understood [17]. *CD24*, a critical breast stem marker, which is lowly expressed in aggressive HER2-positive breast cancer, was also downregulated [18]. We found *DUSP4* to be significantly downregulated, its decreased expression being associated with metastatic cancer [19]. To have a detailed look at individual biological replicates, we plotted a heatmap of the top 30 differentially expressed genes in all samples, which further highlighted the distinct expression patterns between the two cell types (Fig. 2d). We identified a number of novel genes related to lapatinib-acquired drug resistance, including *CSF3R, TLE6, GABRE* and *PAD12*. Additionally, the low expression of *RAP1GAP*, a tumour suppressor gene, whose low expression levels are associated with epithelial-mesenchymal transition (EMT), a phenotype of aggressive cancers [20]. These previously unknown genes could be further validated in physiologically relevant models and may serve as targets for lapatinib-acquired drug resistance in HER2-positive breast cancer.

Our RNA-seq data revealed at least 17 differentially expressed histone-modifying enzymes that play a crucial role in the epigenetic regulation of key cellular functions and the post-translational modification of both histone and non-histone substrates (Fig. 2e). The findings showed significant (p value < 0.05) upregulation of several genes encoding histone deacetylases, including HDAC2, HDAC10 and several lysine demethylases (KDM) enzymes amongst others.

The KEGG pathway analysis indicated that the significantly differentially upregulated genes (adjusted p value < 0.05) were mainly enriched in cell proliferation, angiogenesis and apoptotic process (Fig. 2f). This may imply that these biological processes enhance cell-to-cell contact, potentially leading to increased motility, indicating the ability to acquire new phenotypes for aggressive disease. Additionally, MAPK pathways, multicellular

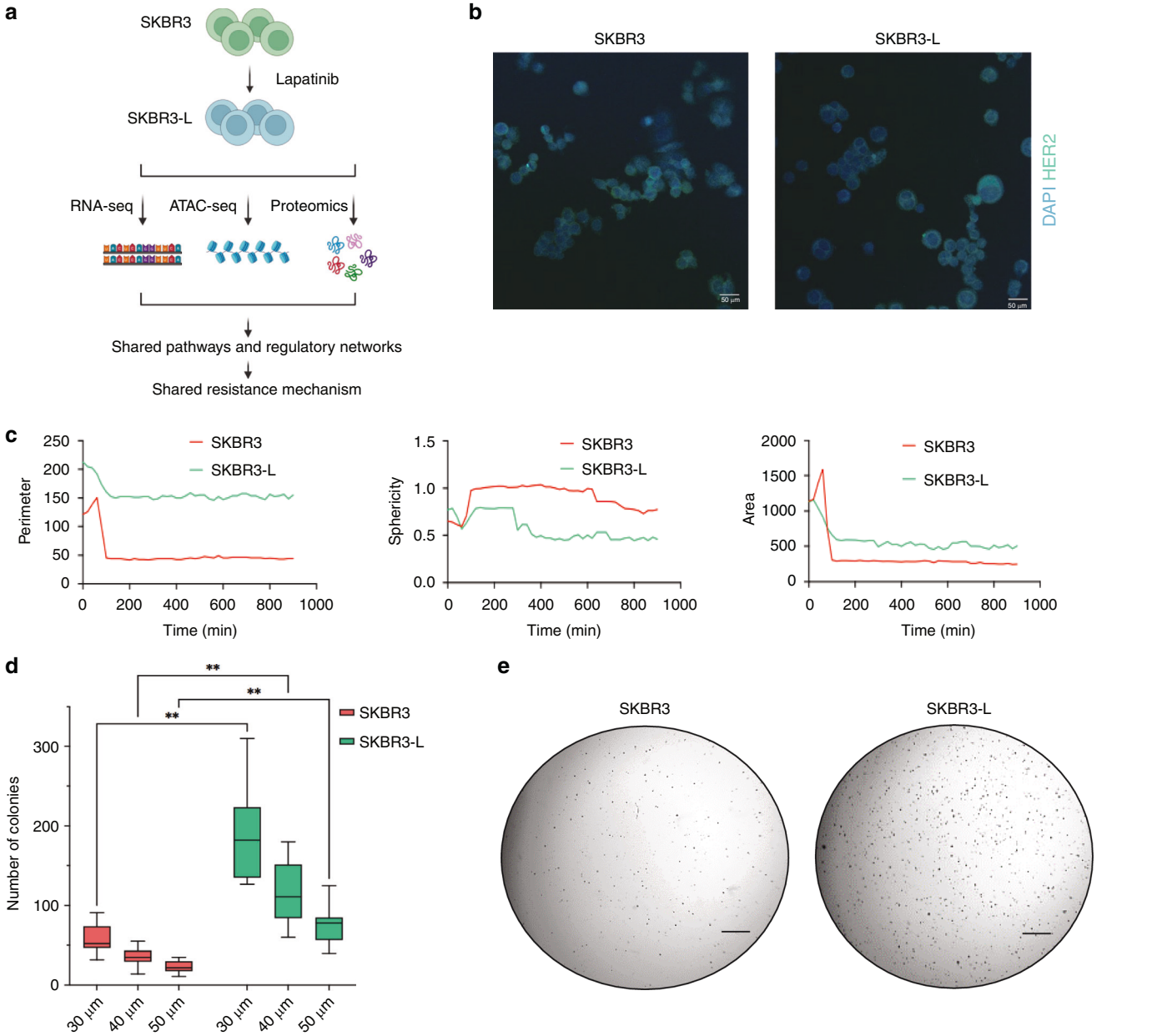

Fig. 1 Phenotypic characteristics of SKBR3 and SKBR3-L cells. a Schematic diagram of the biological model we adapted, and the experimental approaches taken for the duration of the study. SKBR3 cells were made resistant to increasing concentrations of lapatinib. Various functional assays were used to characterise phenotypic changes before multi-omics analysis was performed to identify biomarkers in lapatinib-acquired drug resistance. **b** Fluorescence microscopy confirmed the expression of HER2 protein in both cell types. 20x magnification. Scale bars: 50 µm. **c** Cells were grown in 3D cell cultures and immediately imaged for 15 h. Metrics such as area, sphericity and perimeter were automatically quantified and plotted as line graphs. **d**, **e** Anchorage-independent growth of cells was measured over 3 weeks after cells were grown in 0.35% ultra-pure agarose. Representative microscopic images of colonies stained with crystal violet are shown. Three biological replicates expressed as mean ± SEM. Analysis performed using two-way ANOVA followed by Holm-Šídák post hoc test; $^{**}p < 0.005$. Scale bars: 100 µm.

organism development and oxidation-reduction process indicate engagement of inflammatory responses, which could be a response to cellular stress [21].

ATAC-seq identifies key regions driving lapatinib resistance in breast cancer cells

We used the ATAC-seq to profile the genome-wide accessibility landscape in SKBR3 and SKBR3-L cells. We isolated DNA from SKBR3-L cells and its corresponding lapatinib-sensitive parental cell lines in three biological replicates. Samples exhibited the expected periodicity of the insert length (Supplementary Fig. 1B, C). Hierarchical clustering based on the correlation of accessibility separated the samples into two groups: one containing the majority peaks of SKBR3 samples and the other containing the majority peaks of lapatinib-resistant samples, SKBR3-L (Supplementary Fig. 1D).

We identified 19,854 significantly differential peaks between SKBR3 and SKBR3-L cells with an adjusted p value of <0.05. We conducted a comparison of differential accessible regions (DARs) between these two groups and discovered that SKBR3-L cells showed a decrease in chromatin accessibility with 12,591 peaks indicating lower inaccessibility, as the peaks had a fold-change <0

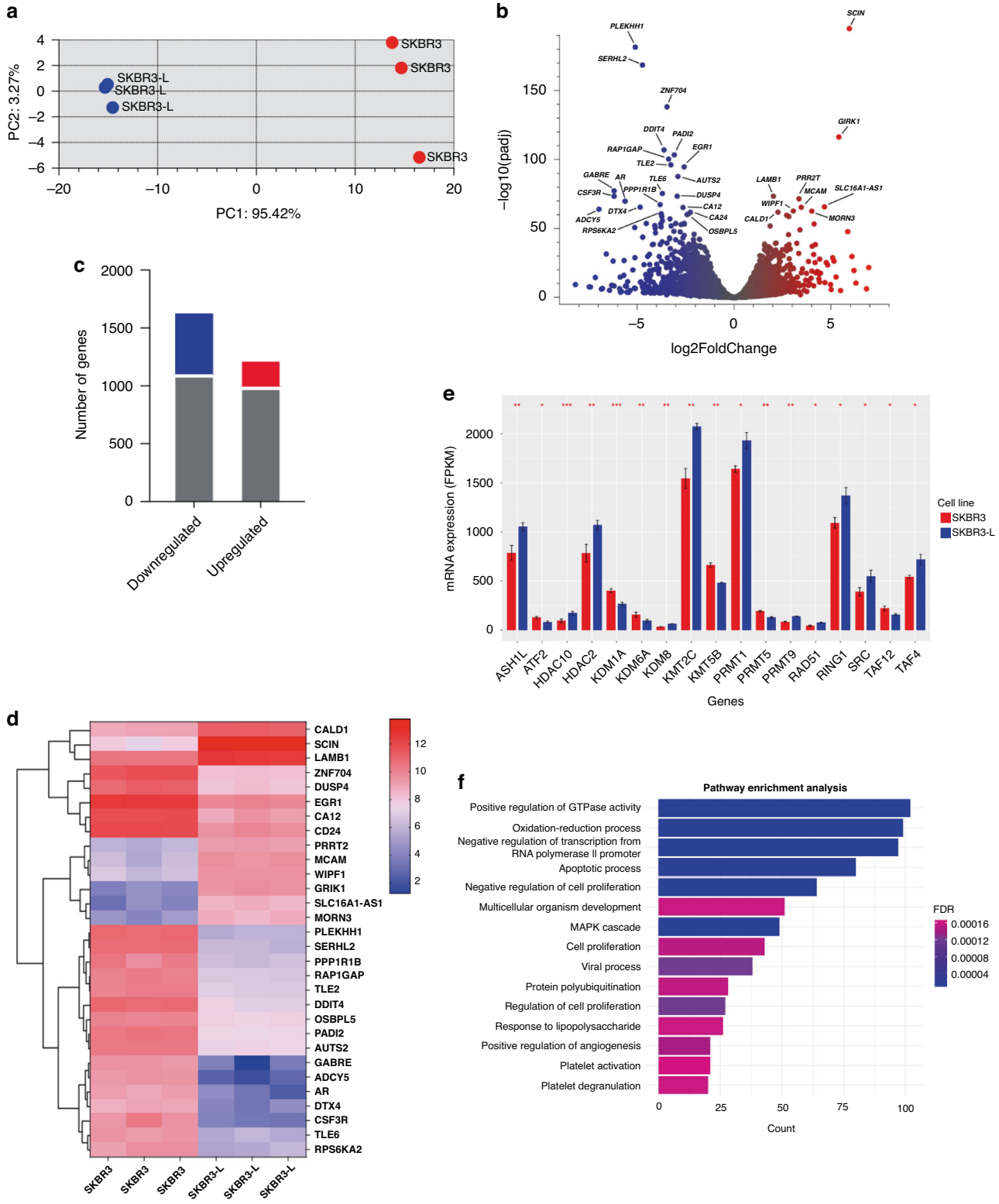

Fig. 2 Differential gene expression between SKBR3 and SKBR3-L cells. a PCA plot displaying variance in gene expression profiles between SKBR3 (red) and SKBR3-L (blue). **b**, **c** Number of differentially expressed genes shown by the volcano plot in SKBR3 compared with SKBR3-L cells, downregulated genes are shown in blue with log2fold change < −2, adjusted *p* value < 0.05. Upregulated genes are shown in red with log2fold change > 2, adjusted *p* value < 0.05. The top 30 significantly differentially expressed genes are labelled. **d** Heatmap of the top 30 significantly differentially expressed genes is shown per individual replicate. **e** Gene expression of the significant epigenetic regulatory genes between SKBR3 and SKBR3-L cells. **f** Biological pathways associated with significantly differentially expressed genes. For all this analysis, three biological replicates are expressed as mean ± SEM; **p* < 0.05, ***p* < 0.005, ****p* < 0.0005.

with an adjusted p value < 0.05. Seven thousand two hundred sixty-one peaks showed accessibility with a fold-change >0 and an adjusted p value < 0.05. We observed 1213 regions as 'hyper-accessible' (>2-fold-change, adjusted p value < 0.05) and 1914 regions as 'hypo-accessible' (<2-fold-change, adjusted p value < 0.05) (Fig. 3a and Supplementary Fig. 1D). Through further quantitative comparison of the two cell types, we identified the resistant cell line to have greater inaccessibility with concentration changes at the higher end (≥8) reducing from 4106 regions to 3085 regions and the lower end (2–3.99) increasing from 911 regions to 1192 (Supplementary Fig. 2A).

A hierarchical clustered heatmap was produced to visualise the expression profile of the top 30 DARs corresponding to the accessibility signal, sorted by their log2fold change of >0.5, adjusted p value < 0.05 through plotting their log2-transformed expression change value (Fig. 3b). Through this, we were able to identify and visualise co-regulated regions across treatment conditions. Through the linkage of known gene regions and chromatin states, we confirmed *EGFR* to be highly accessible, known to give cells basal-like features [22]. In addition, *SCIN*, a gene strongly associated with proliferation, migration and differentiation in cancer, exhibited with a (log2fold change of 7.52) high level of significance. *TRIP13* and *IGF2BP3*, which promote tumour growth, were also highly differentially accessible [23, 24]. Furthermore, we observed downregulation of AJAP1 expression, which has previously been implicated in promoting distant metastasis through the Wnt signalling pathway [25]. Although CDCP1 and ACL8 expression is also reduced in SKBR3-L cells, their low expression has been associated with favourable outcomes in cancers [25, 26].

TFs regulate gene expression by binding to specific DNA sequences in promoter regions [21]. Chromatin accessibility is crucial for TF binding as it impacts the TF's ability to bind to the nucleosomes [22]. Using ATAC-seq data and HOMER v.4.11 for motif enrichment analysis, we identified candidate TFs associated with genomic alterations by analysing differential chromatin accessibility in promoter or enhancer elements.

Our analysis identified 444 known motifs enriched with 27 de novo results that showed significant enrichment (adjusted p value < 0.05). We found the ERG motif to be highly enriched alongside FOXM1, an oncogenic TF known to be highly upregulated in breast cancer and associated with poor patient survival, which was significantly enriched in accessible regions (Fig. 3c) [27]. Additionally, we identified several Zinc Finger family members, which include the Kruppel-like factor (KLF) family members, to be significantly enriched, followed by others from Erythroblast Transformation Specific, basic Helix-Loop-Helix and Forkhead box (Fox). Each TF's enrichment was quantified, with the most significant log10 > 50, adjusted p value < 0.05.

Furthermore, we categorised the differential peak analysis to each chromosome to assess the distribution of chromatin dynamics across the genome (Fig. 3d). The accessibility of the chromosomes varies, with chromosome 4 showing the greatest increase in accessibility at 138 'hyper-accessible' regions identified. Aberrations in chromosome 4 are associated with several types of cancers, for which 141 tumours secreted and 54 cancer-associated proteins are encoded, revealing regions in chromosome 4 as a strong candidate for biomarker verification and drug target discovery research [28].

Furthermore, genomic annotation of DARs revealed a clear distribution pattern with 435 hyper-accessible regions predominantly located in gene-distal intergenic areas, these likely control the spatiotemporal and quantitative expression dynamics and activation of potential enhancer that affect transcriptional activity (Supplementary Fig. 2B). In contrast, 743 hypo-accessible regions were found within intron regions and aberrant intron retention has high association with several cancer types [29]. Overall, we identified 3888 regions with differential accessibility at or near the Transcription Start Site (TSS) (1 kbp), of which 72.6% coincided with RNA-seq data, confirming chromatin accessibility's role in modulating gene expression.

Following differential peak analysis, the top 100 significant regions were extracted and filtered by TSS distance and those within 6 base pairs of the TSS had their chromatin landscape mapped. In total, 15 out of the 100 significant regions were at or near the TSS. Genes identified included novel genes such as *HPGD, FASN and KRT81*, as well as *SCIN* and *TPM1* which have already been confirmed in acquired drug resistance mechanisms associated with HER2-positive breast cancer (Fig. 3e). These genomic regions may not only provide an understanding of how the chromatin accessibility landscape may contribute to different treatment response, but also aid in our understanding of how epigenetic/transcriptomic mechanisms may influence drug sensitivity and resistance [30, 31]. These regions could prove to be potential targets for future investigation for their role in drug resistance.

Proteomic analysis confirmed markers identified in transcriptomic datasets

To interrogate the dynamic changes at the proteome level, we performed an unbiased proteomic analysis using liquid chromatography–tandem mass spectrometry (LC-MS/MS) between SKBR3 and SKBR3-L cells. In total, we identified 325 proteins with significant increased expression, log2fold change > 0.1, adjusted p value < 0.05 and 270 with significantly decreased expression, log2fold change < −0.1, adjusted p value < 0.05 (Fig. 4a). All proteins quantified in each cell type were visualised in a volcano plot depicting protein abundance changes between SKBR3 and SKBR3-L cells (Fig. 4b). The differentially expressed proteins were clustered and visualised as each biological replicate on a heatmap (Fig. 4c). Proteins within each cell type are clustered together and show consistent expression patterns.

We further visualised the protein expression change of the top 15 upregulated and top 15 downregulated proteins in a bar graph (Fig. 4d) for comparison. We found RCN1, TRIP6 and HPGD to be amongst those significantly upregulated, confirming some of the candidates we observed in our RNA-seq and ATAC-seq datasets. Whilst AFMID, CD59 and KRT81 to be significantly downregulated. PROM2 was amongst those downregulated and is of significant interest as its prognostic value in cancer is controversial, with its underexpression potentially providing benefit to drug-resistant cells [32].

Pathway enrichment analysis of both significantly (adjusted p value < 0.05) upregulated and downregulated proteins confirmed pathways identified in RNA-seq (Fig. 2f) were also identified in proteomic (Fig. 4e). Upregulated pathways showed enrichment of proteins implicated in the EMT process. Additionally, double-strand break repair was also enriched, which contributes to genomic instability. KRAS signalling, which is highly intertwined with HER2 signalling, plays a key role in cell survival, proliferation and migration. Downregulated pathways included extracellular exosome—small extracellular vesicles that play a role in cell-to-cell communication and mTORC1, which is involved in signal integration from multiple growth factors and energy supplies to promote cell growth [33].

A combined approach to unravelling resistance culminates in nine candidate markers

To unravel the complex interactions and resistance mechanisms between SKBR3 and SKBR-L cells, we employed an integrated multi-omic approach, combining ATAC-seq, RNA-seq and proteomics data. This comprehensive data analysis led to the identification of 83 significant differential changes (showcased in a Venn diagram), revealing shared genomic regions that could be key targets for future research (Fig. 5a). We further dissected these interactions using volcano plots, providing a detailed view of the

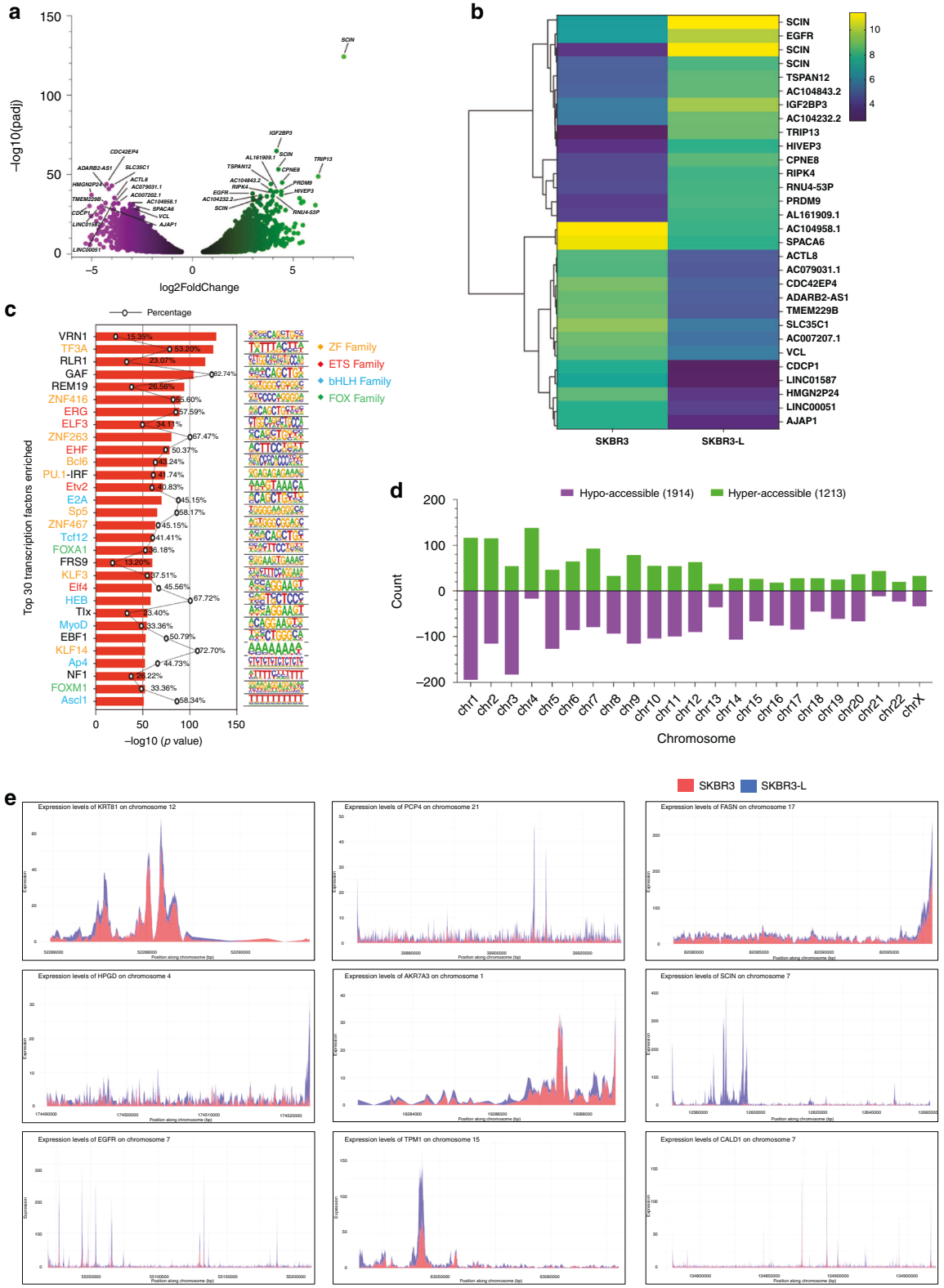

Fig. 3 Chromatin accessibility changes between SKBR3 and SKBR3-L cell lines. a Volcano plot of differentially accessible regions with the top 30 significant regions labelled by gene, with log2fold change < −2, adjusted *p* value < 0.05 (purple). Upregulated regions are shown with log2fold change > 2, adjusted *p* value < 0.05 (green). **b** Hierarchical clustered heatmap of the top 30 significantly differentially expressed regions identified by gene. **c** Transcription factor enrichment motif analysis. Top 30 significant hits (adjusted *p* value < 1e-52) identified motifs and the transcriptional factors that bind to the region. **d** Comparison by chromosome of SKBR3 SKBR3-L cell lines. Hyper-accessible regions (log2fold change > 2, adjusted *p* value < 0.05) and hypo-accessible regions (log2fold change < −2, adjusted *p* value < 0.05) are plotted on the bar graph. **e** Candidate regions within 6 bp from the TSS of nine different markers between SKBR3 and SKBR3-L cells. SKBR3 (red), SKBR3-L (blue).

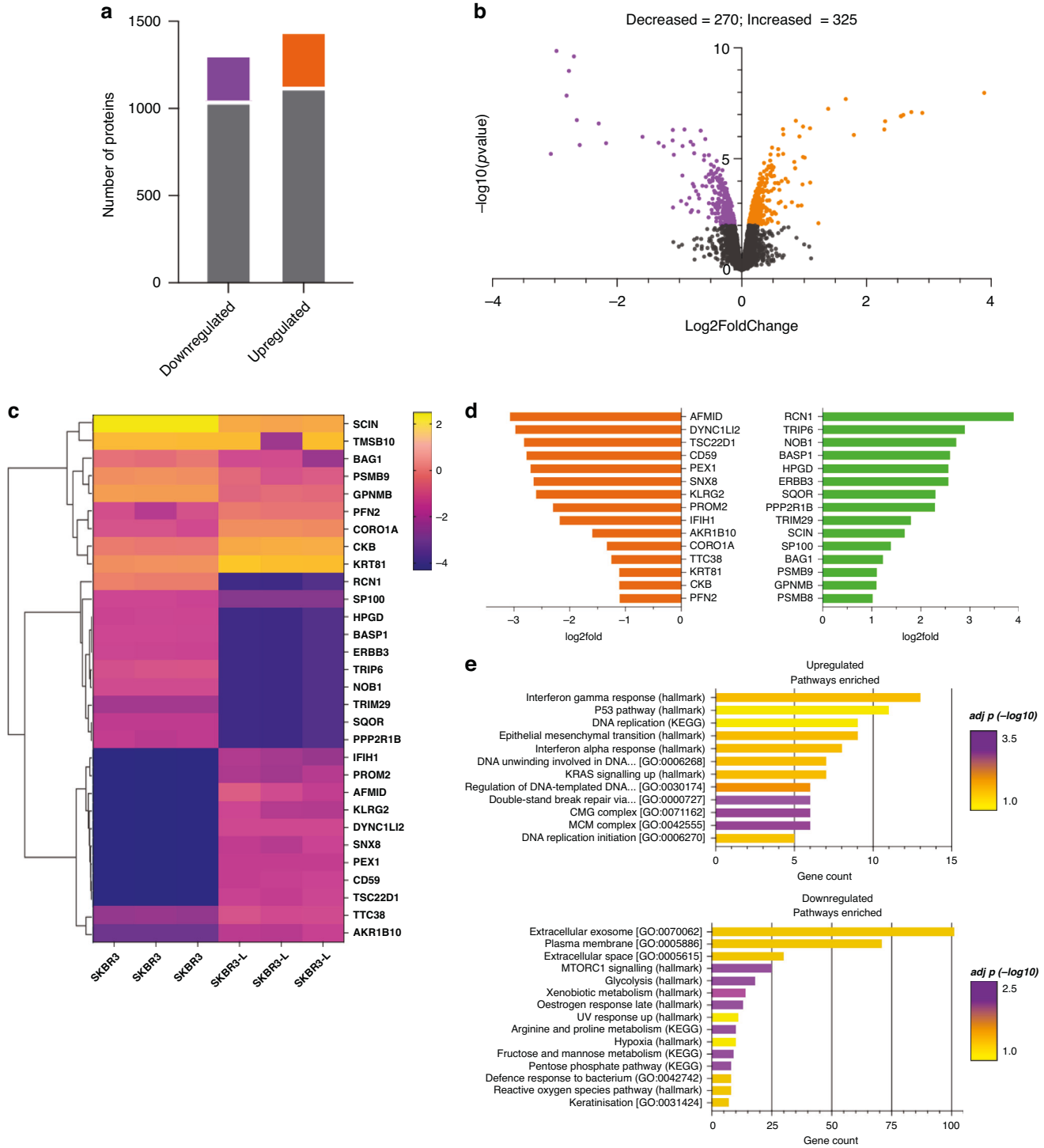

Fig. 4 Proteomic analysis validated the markers found in transcriptomic datasets. a Number of differentially expressed proteins in SKBR3 compared with SKBR3-L cells. Statistical significance is shown as log2fold change > 2, adjusted *p* values < 0.05 for upregulated proteins and log2fold change < −2, adjusted *p* values < 0.05 for downregulated proteins. **b** Volcano plot of differentially expressed proteins between SKBR3 and SKBR-L cells. **c** Heatmap of the top 30 significantly differentially expressed genes labelled for each biological replicate. **d** Bar plot showing the top 15 downregulated and upregulated proteins based on their log2fold expression. **e** Bar plot showing biological pathways associated with significantly differentially expressed proteins (adjusted *p* value < 0.05).

relationships between differentially expressed genes, accessible chromatin regions and proteins (Fig. 5b).

Focusing on key candidate markers in the three datasets, we narrowed down our list to nine markers with significant changes across ATAC-seq, RNA-seq and proteomic data, suggesting their potential roles in the development of lapatinib resistance. These markers were visualised using a hierarchical clustered heatmap, which displayed the co-regulated expression patterns across different treatment conditions in the three datasets (Fig. 5c). Notably, genes such as *SCIN* and *EGFR*, already known to be involved in HER2-positive breast cancer, were confirmed, reinforcing the validity of our approach. Other significant novel

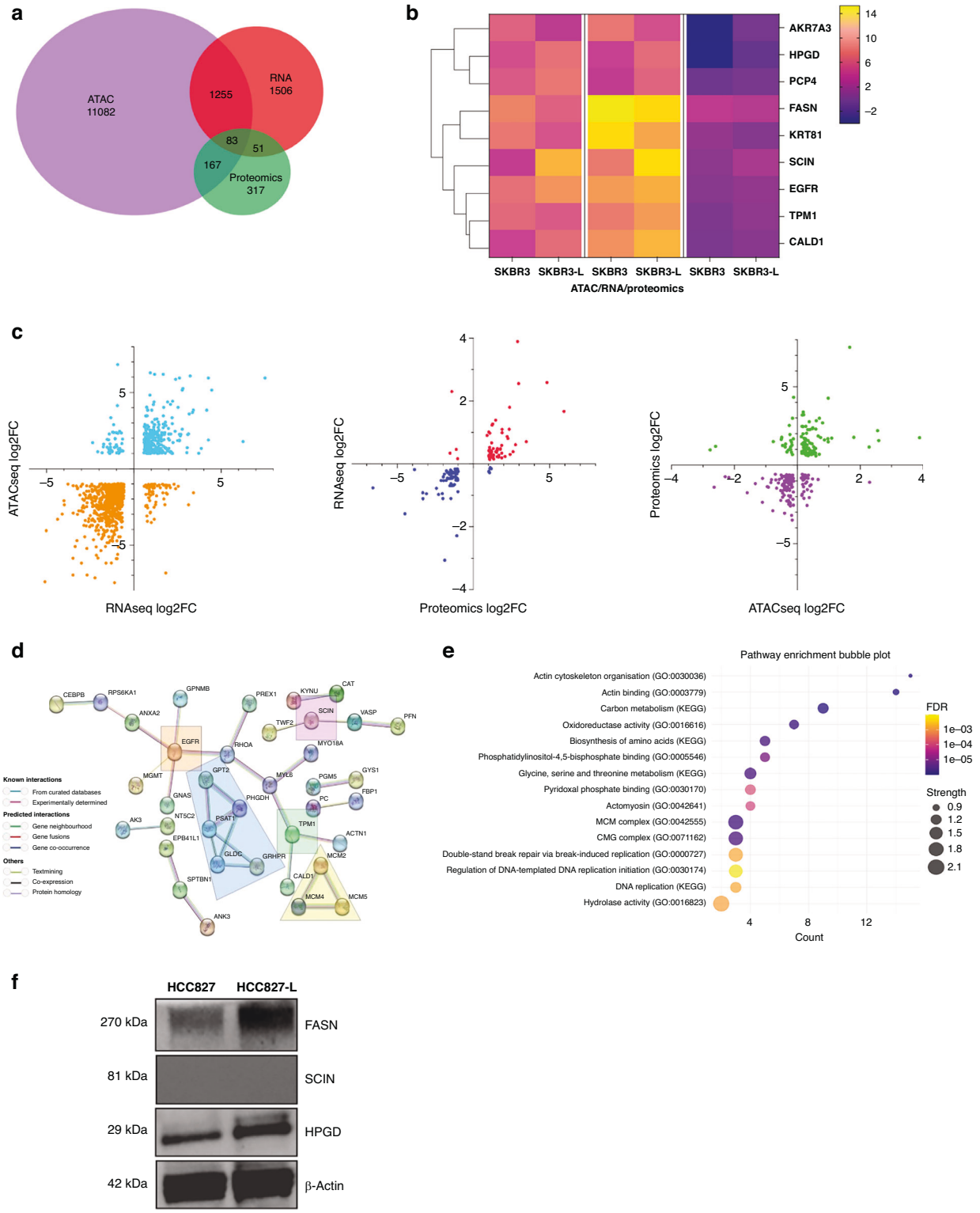

Fig. 5 A combined approach to investigating lapatinib resistance resulted in the identification of nine candidate markers. a Overlapping regions between ATAC-seq (log fold-change > 1, adjusted p value < 0.05), RNA-seq (log fold-change > 1, adjusted p value < 0.05) and proteomics (log fold-change > 0.1, adjusted p value < 0.05). **b** Heatmap of nine candidate genes identified as differentially expressed/accessible across the three datasets. **c** Volcano plots of significantly differentially regulated interactions showing RNA-seq vs ATAC-seq, proteomics vs RNA-seq, ATAC-seq vs proteomics. **d** Protein-protein interaction network. The markers encoded by the common 83 identified genes as identified in the three datasets. Analysed with String v.12.0 and mapped; nodes indicating proteins and different coloured edges representing protein-protein associations amongst neighbouring nodes. **e** Biological pathways associated with the 83 significantly differentially expressed genes as observed in the three datasets. **f** Western blot analysis confirmed increased protein expression of HPGD and FASN in lapatinib-resistant HCC827-L cells compared to the parental HCC827 cells, indicating upregulation of both proteins upon acquisition of resistance in a different model.

candidate genes include *HPGD*, *TPM1*, *CALD1*, *PCP4*, *AKR7A3*, *KRT81* and *FASN*, which are anticipated to be pivotal in lapatinib-resistant mechanisms.

To reveal the protein-protein interaction (PPI) network and co-expression of the differential expressed proteins identified in our integrated analysis (adjusted p value < 0.05), we utilised String v.12.0 to analyse known and predicted physical interactions and functional associations between proteins (Fig. 5d). We used a high co-expression/interaction base score (0.700) to ensure high accuracy, and our PPI enrichment returned an overall p value of 0.0000137 with an average local cluster coefficient of 0.327. Proteins such as EGFR and TPM1 are centrally located and have multiple connections displayed within the network, suggesting their key role in driving lapatinib-acquired drug resistance.

A pathway enrichment analysis of the 83 significant proteins (Fig. 5e) revealed significant enrichment (adjusted p value < 0.05) in pathways related to actin remodelling, carbon metabolism and double-strand break repair. Actin remodelling influences tumour growth and chemoresistance, with aberrant actin isoforms serving as cancer biomarkers [34]. Carbon metabolism plays a role in tumorigenesis and drug resistance via DNA methylation, while impaired double-strand break repair contributes to genomic instability [35]. To validate the expression of key biomarkers identified in our multi-omics analysis, we selected three of the most differentially expressed candidates from the integrated dataset for western blot analysis. These experiments were conducted in the HCC827 lung cancer cell line, which we rendered resistant to lapatinib (HCC827-L) through gradual drug exposure. Of the three biomarkers tested—FASN and HPGD—showed clear upregulation in the lapatinib-resistant cells compared to the parental HCC827 line. Notably, this validation was performed in a completely independent model system, distinct from the original SKBR3 breast cancer cells. These findings support the relevance of these biomarkers in mediating lapatinib resistance across different cancer types.

DISCUSSION

Acquired drug resistance is a high probability event in breast cancer in which cancer cells must remodel and rewire their genome, epigenome and proteome to be able to evade treatment and molecularly evolve into an incurable disease. Despite advancements in targeted therapies like lapatinib, drug resistance in HER2-positive breast cancer persists, with over 70% of patients relapsing after initial treatment [1]. This high frequency of acquired drug resistance in breast cancer cells could highlight their inherent ability to relapse. In contrast, our work shows that HER2-positive breast cancer cells gain the ability to become resistant to lapatinib through the dramatic remodelling of the chromatin, transcriptome and the proteome (Fig. 5b, c). Surprisingly, our data demonstrate that the aggressive phenotype observed in drug resistance correlates with downregulation in gene expression patterns and condensed chromatin landscape associated with limited, yet robust changes in the proteome. Our findings showcase the strength of integrating genome-wide molecular techniques using a genetic model system to reveal previously unnoticed variations in cellular states across multiple levels of regulation.

Across many cancer types, increased chromatin accessibility [36, 37] and gene expression changes correlate with aggressiveness and poor patient outcomes [38]. However, in our in vitro model, the link between increased chromatin accessibility and aggressiveness was not observed, as our investigation revealed a predominant decrease in chromatin peaks associated with significant downregulation of gene expression, suggesting a reduction of accessibility was associated with resistance mechanisms. Our data indicate that when developing lapatinib-acquired drug resistance, cells establish an invasion-promoting gene expression programme through stabilising chromatin dynamics at specific regulatory genes. AKR7A3, a member of the aldo-keto reductase (AKR) protein family, is downregulated in SKBR3-L cells (Figs. 3e and 5b). Its downregulation is associated with metastasis in pancreatic ductal carcinoma [39]. We observed elevated expression in other key regions, such as EGFR and SCIN, which are well-known to be highly expressed in breast cancer resistance. We saw significant transcriptional changes including the downregulation of key markers like EGR1 and CD24, whose reduced expression is linked to increased invasiveness and drug resistance and identified proteins such as TRIP6 and TRIM29 that enhance (cancer stem cells) CSC-like properties [40, 41]. Our analysis identified nine candidates (Figs. 3e and 5b, c) that were significantly differentially expressed across all three datasets, including seven novel candidates, as being involved in drug resistance in HER2-positive breast cancer. We think that, despite the predominant chromatin closing and the corresponding downregulation of gene expression with minimal proteome changes, certain key regulatory elements undergo significant shifts during acquired drug resistance. These changes likely drive the phenotypic alterations in drug resistance observed in our in vitro model. Chromatin closing results in the downregulation of genes linked to disruptive changes in cell morphology and motility (Fig. 1c–e). Meanwhile, other regions with differentially accessible chromatin suggest network rewiring, contributing to the development of an aggressive phenotype during acquired drug resistance.

Our data suggests that SKBR3-L cells exist in a 'pre-emptive' chromatin configuration state that has an overall inaccessible chromatin dynamic, which still permits the binding of specific motifs during drug resistance. Our results show the enrichment of several TFs, particularly pioneer factors such as Foxa, KLF and Ascl1 (Fig. 3c). These enriched motifs could establish this 'pre-emptive' architecture that binds their target sites in closed chromatin and subsequent chromatin opening (Figs. 3e and 5c) [42]. This could explain the pattern of overall chromatin closing in SKBR3-L cells being observed concurrently with enhanced accessibility near the transcriptional start site, particularly within six base pairs of critical genes involved in drug resistance.

The aggressive nature of lapatinib-resistant cells is evident compared to their cancer counterpart, as our analysis shows significant anchorage-independent growth (Fig. 1d), which correlates with hyperactivation of the MAPK and KRAS pathways (Figs. 2f and 4e), leading to an enhanced transformational potential (Fig. 1d, e) [43]. Upregulation of upstream receptors, such as HER2 and EGFR—key activators of the MAPK pathway, also contributes to enhanced growth and drug resistance [44–46]. Additionally, morphological changes, including loss of sphericity and increased overall cell size (Fig. 1c), suggest a loss of cell-to-cell contact and communication, indicative of invasive behaviour. This is consistent with our PPI analysis, where pathways related to cytoskeletal organisation and cell adhesion were highly enriched (Fig. 5f). These alterations are often associated with a transition to a mesenchymal phenotype (Fig. 4e), which is characterised by increased motility, invasiveness and drug resistance, which are features of the metastatic state [47].

While the gene expression patterns of lapatinib-sensitive cells at the baseline level displayed some diversity between biological replicates, cells that developed drug resistance exhibited a notable convergence in their expression profiles (Fig. 2a). This uniformity in adaptive responses among the resistant cells is potentially due to the selective pressure of lapatinib with resistant cells activating similar pathways that lead to a stabilisation of specific gene expression patterns. A significant proportion (~46%) of transcriptional changes coincided with significant chromatin alterations (Fig. 5a). Alongside this, a notable overall decrease in gene expression patterns correlated with genes showing closed chromatin states at the promoter region in the resistant cell line,

underscoring the epigenome's role as a regulator of resistance in HER2-positive breast cancer. From an epigenetic regulation standpoint, we examined changes in the expression of known epigenetic enzymes (Fig. 2e). The findings indicate that the upregulation of HDACs may play a role in the downregulation of specific genes associated with lapatinib resistance. Previous studies have explored the epigenomic context of trastuzumab resistance, with hypermethylation of MCF7 cells being identified as a driver of resistance; nonetheless, few studies have emerged on SKBR3 cell lines, which are associated with a more invasive and aggressive phenotype [48, 49].

We took a target discovery approach using a combined molecular analysis, which led to the identification of a lapatinib-acquired drug resistance-signature (Fig. 5b), serving as a potential target for reversing drug resistance. These target genes and their associated pathways not only shed light on the mechanistic underpinnings of drug resistance but also highlight the complex interplay between genetic and epigenetic factors in cancer progression. The use of a multi-omics approach has recently emerged as a promising technique to identify previously unknown drug targets. Given the dramatic remodelling of the key gene regulatory state as a result of changes in the chromatin, which leads to changes in gene expression and proteins, we speculate that other cancer types may also have a similar signature as we have observed. Our target discovery approach provides the scientific community future research incentive to study this signature in models that are physiologically relevant to the human context, and if confirmed, to target it with inhibitors and gene manipulation technologies as a basis for potential biomarkers in acquired drug resistance.

METHODS

Cell culture

The SKBR3 and SKBR3-L cell lines were gifted by [6] and grown under recommended conditions. Briefly, SKBR3 and SKBR3-L cell medium consists of McCoy's 5A Medium (ThermoFisher, #16600082) supplemented with 5% horse serum (Sigma-Aldrich, #H1138) and 1× penicillin/streptomycin (Pen/Strep). The SKBR3-L cells were cultured in 2 µM Lapatinib (BioTechne, #6811/10).

SKBR3 cells were cultured in increasing concentrations of lapatinib, starting approximately from the IC50 value, respectively 77 nM, as determined by dose-response studies. Through continuous exposure to the drug, the lapatinib-sensitive cells die and the live cells are cultured until they outgrow the lapatinib dose. The dose is increased, and the process is repeated until the cells are able to grow in 2 µM of lapatinib, a concentration equal to twice the resistance threshold.

3D cell culture and morphology analysis

3D cell culture was performed using pre-made BIO-FLOAT 96-well plates (Sarstedt, #83.3925.400) with a round base. 1000 cells were plated onto the 96-well plates and cells/spheroids were immediately visualised and tracked using LiveCyte2 quantitative phase imaging (QPI) for 12 h to characterise the changes in morphology. Morphological changes were analysed using software (Acquire) embedded in the microscope and metrics such as size, area and motility were processed.

Immunofluorescence assays

Cells were fixed with 4% paraformaldehyde (PFA), permeabilised using 0.5% Triton X-100 and blocked with 10% goat serum in PBS containing Tween-20 (PBS-T). They were then incubated with the HER2 antibody (Cell Signalling, #2165) for 2 h at room temperature. Following staining, the detachable chambers were removed, and the cells were mounted using mounting medium and left to dry in the dark at room temperature. Once dry, the slides were imaged using a fluorescence microscope.

Soft agar colony formation assay

A 0.8% base layer mixed with cell medium was formed in plates using ultra-pure culture-grade agarose (Thermo Fisher Scientific, #16500500), allowed to solidify at room temperature for 30 min. 5000 cells per well were mixed with 0.35% ultra-pure agarose with cell medium and plated evenly, drop-wise, on top of the bottom layer for overlay culture. Medium was changed every 3 days for 3 weeks. Colonies were fixed using 4% PFA and permeabilised using 100% methanol. Colonies were stained using 0.05% Crystal Violet dye (APC Pure, #RRSP23-D), and images were taken using a brightfield microscope (Nikon Ni-E, fitted with the Nikon DS-Fi3 camera), capturing most of the perimeter of the well. Binary masks were applied to each of the images, and thresholding parameters for a diameter ranging from 30 to 50 µm were set on ImageJ. Colonies were counted using ImageJ only if they satisfied the criteria above the threshold values, and colony counts were then manually checked and adjusted if necessary.

RNA extraction, library preparation and NovaSeq sequencing

Total RNA was extracted from frozen cell pellets using Qiagen RNeasy Mini kit following the manufacturer's instructions (Qiagen, Hilden, Germany). RNA samples were quantified using Qubit 4.0 Fluorometer (Life Technologies, Carlsbad, CA, USA) and RNA integrity was checked with RNA Kit on Agilent 5300 Fragment Analyser (Agilent Technologies, Palo Alto, CA, USA). RNA sequencing libraries were prepared using the NEBNext Ultra RNA Library Prep Kit for Illumina following the manufacturer's instructions (NEB #E7770, Ipswich, MA, USA). Briefly, mRNAs were first enriched with Oligo(dT) beads. Enriched mRNAs were fragmented for 15 min at 94 °C. First-strand and second-strand cDNAs were subsequently synthesised. cDNA fragments were end-repaired and adenylated at 3′ends, and universal adaptors were ligated to cDNA fragments, followed by index addition and library enrichment by limited-cycle PCR. Sequencing libraries were validated using the NGS Kit on the Agilent 5300 Fragment Analyser (Agilent Technologies, Palo Alto, CA, USA) and quantified by using Qubit 4.0 Fluorometer (Invitrogen, Carlsbad, CA). The sequencing libraries were multiplexed and loaded on the flowcell on the Illumina NovaSeq instrument according to the manufacturer's instructions. The samples were sequenced using a 2 × 150 Pair-End (PE) configuration v1.5. Image analysis and base calling were conducted by the NovaSeq Control Software v1.7 on the NovaSeq instrument. Raw sequence data (.bcl files) generated from Illumina NovaSeq were converted into fastq files and de-multiplexed using the Illumina bcl2fastq programme version 2.20. One mismatch was allowed for index sequence identification.

Data analysis of RNA-seq

After investigating the quality of the raw data, sequence reads were trimmed to remove possible adaptor sequences and nucleotides with poor quality using Trimmomatic v.0.36. The trimmed reads were mapped to the Homo sapiens reference genome available on ENSEMBL using the STAR aligner v.2.5.2b. The STAR aligner is a splice aligner that detects splice junctions and incorporates them to help align the entire read sequences to generate BAM files. Unique gene hit counts were calculated by using feature Counts from the Subread package v.1.5.2. Only unique reads that fell within exon regions were counted. After the extraction of gene hit counts, the gene hit counts table was used for downstream differential expression analysis. Using DESeq2, a comparison of gene expression between the groups of samples was performed. The Wald test was used to generate p values and Log2 fold changes. Genes with adjusted p values ≤ 0.05 and absolute log2fold changes ≥ 1 were identified as differentially expressed genes for each comparison. A gene ontology analysis was performed on the statistically significant set of genes by implementing the software GeneSCF v.1.1. The goa_human GO list was used to cluster the set of genes based on their biological process and determine their statistical significance. A PCA analysis was performed using the 'plotPCA' function within the DESeq2 R package. The plot was created in Graphpad Prism v.10.0.3 and shows the samples in a 2D plane spanned by their first two principal components. The top 500 genes, selected by highest row variance, were used to generate the plot. Subsequent plots and graphs were produced using R v.4.4.0 and GraphPad Prism v.10.0.3.

ATAC-seq library preparation and sequencing

Live cell samples were quantified and assessed for viability using a Countess Automated Cell Counter (ThermoFisher Scientific, Waltham, MA, USA). After cell lysis and cytosol removal, nuclei were treated with Tn5 enzyme (Illumina, #20034197) for 30 min at 37 °C and purified with Minelute PCR Purification Kit (Qiagen, #28004) to produce tagmented DNA samples. Tagmented DNA was barcoded with Nextera Index Kit v2 (Illumina, #FC-131-2001) and amplified via PCR prior to a SPRI Bead cleanup to yield purified DNA libraries. The sequencing libraries were clustered on a NovaSeq flowcell. After

clustering, the flowcell was loaded on the Illumina NovaSeq instrument according to the manufacturer's instructions. The samples were sequenced using a 2 × 150 bp Paired End (PE) configuration. Image analysis and base calling were conducted by the Control Software (CS). Raw sequence data (.bcl files) generated from the Illumina instrument were converted into fastq files and de-multiplexed using Illumina's bcl2fastq 2.17 software. One mismatch was allowed for index sequence identification.

Data analysis of ATAC-seq

After investigating the quality of the raw data, sequencing adaptors and low-quality bases were trimmed using Trimmomatic 0.38. Cleaned reads were then aligned to the reference genome GRCm38 using bowtie2. Aligned reads were filtered using samtools 1.9 to keep alignments that (1) have a minimum mapping quality of 30, (2) were aligned concordantly and (3) were the primary called alignments. PCR or optical duplicates were marked using Picard v.2.18.26 and removed. Prior to peak calling, reads mapping to mitochondria (mt) were called and filtered, and reads mapping to unplaced contigs were removed. MACS2 v.2.1.2 was used for peak calling to identify open chromatin regions. Valid peaks from each group or condition were then merged and peaks called in at least 66% of samples were kept for downstream analyses. For each pair-wise comparison, peaks from SKBR3 and SKBR3-L were merged, and peaks found in either condition were kept for downstream analyses. Reads falling beneath peaks were counted in all samples, and these counts were used for differential peak analyses using the R package DiffBind v.3.14. BED files were then loaded into HOMER v.5.0 for MOTIF enrichment analysis and the top 30 known TFs identified. Plots and graphs were produced using R v.4.4.0 and GraphPad Prism v.10.0.3.

Proteomic sample preparation

For proteomic experiments, cells were grown in 2D cell cultures. Thirty micrograms of protein were subjected to cysteine reduction and alkylation using sequential incubation with 10 mM dithiothreitol and 16.6 mM iodoacetamide for 1 h and 30 min, respectively, at 25 °C with agitation. Trypsin beads (50% slurry of TLCK-trypsin) were equilibrated with three washes with 20 mM HEPES (pH 8.0). The urea concentration in the protein suspensions was reduced to 2 M by the addition of 600 µL of 20 mM HEPES (pH 8.0) and 70 µL of equilibrated trypsin beads were added and the samples were incubated overnight at 37 °C. Trypsin beads were removed by centrifugation (2000 × *g* at 5 °C for 5 min).

Peptide solutions were desalted using the AssayMAP Bravo (Agilent Technologies) platform. For desalting, the protocol peptide clean-up v3.0 was used. Reverse phase S cartridges (Agilent, 5 µL bed volume) were primed with 250 µL 99.9% acetonitrile (ACN) with 0.1%TFA and equilibrated with 250 µL 0.1% TFA at a flow rate of 10 µL/min. The samples were loaded at 20 µL/min, followed by an internal cartridge wash with 0.1% TFA at a flow rate of 10 µL/min. Peptides were then eluted with 105 µL of solution (70/30 ACN/H_2O + 0.1% TFA). Eluted peptide solutions were dried in a SpeedVac vacuum concentrator and peptide pellets were stored at −80 °C.

Samples were processed and run in the mass spectrometry on consecutive days in order to reduce technical variability. Peptide pellets were reconstituted in 5 µL of 0.1% TFA, 2 µL of this solution were further diluted in 18 µL of 0.1% TFA and 2 µL were injected into the LC-MS/MS system. The LC-MS/MS platform consisted of a Dionex Ultimate 3000 RSLC coupled to a Q Exactive™ Plus Orbitrap Mass Spectrometer (Thermo Fisher Scientific) through an EASY-Spray source. Mobile phases for the chromatographic separation of the peptides consisted of Solvent A (3% ACN; 0.1% FA) and Solvent B (99.9% ACN; 0.1% FA). Peptides were loaded in a µ-pre-column and separated in an analytical column using a gradient running from 3 to 28% B over 90 min. The UPLC system delivered a flow of 10 µL/min (loading) and 250 nL/min (gradient elution). The Q Exactive Plus operated a duty cycle of 2.1 s. Thus, it acquired full scan survey spectra (*m/z* 375–1500) with a 70,000 FWHM resolution, followed by data-dependent acquisition in which the 15 most intense ions were selected for HCD (higher energy collisional dissociation) and MS/MS scanning (200–2000 *m/z*) with a resolution of 17,500 FWHM. A dynamic exclusion period of 30 s was enabled with a *m/z* window of ±10 ppm. Mass spectrometry data collection was carried out using Thermo Scientific FreeStyle 1.4.

Data analysis for proteomics

MS raw files were converted into mzML using MSConvert, part of the ProteoWizard software package [5]. FragPipe (version v22.0) [6] with MSFragger (version 4.1) [7], Percolator (3.07.01) [7] and PTM-Shepherd (v2.0.5) [8] to analyse the data. Peptide and phosphopeptide quantification were performed using in-house software Pescal as described before [3]. The resulting quantitative data was further analysed using the Protools 2 R package(https://github.com/CutillasLab/protools2/releases/tag/v0.2.12.)

Statistical analysis

R v.4.4.0 [programming language] and GraphPad Prism v.10.0.3 were used for statistical analysis. This included data refinement, transformations, normalisations and descriptive statistics. Alongside this, R v.4.4.0 and GraphPad Prism v.10.0.3 were also used to illustrate our findings, utilising an array of heatmaps, dendrograms, volcano plots, bubble plots and bar graphs. Experiments were all carried out in triplicates, and the False Discovery Rate was used to control type 1 error, ensuring high accuracy in our findings.

DATA AVAILABILITY

The BioProject ID for the RNA-seq and ATAC-seq data reported in this paper is: PRJNA1170334. The mass spectrometry-based proteomics data have been deposited to the ProteomeXchange Consortium via the PRIDE Project accession: PXD056848.

REFERENCES

1. Yang J, Ju J, Guo L, Ji B, Shi S, Yang Z, et al. Prediction of HER2-positive breast cancer recurrence and metastasis risk from histopathological images and clinical information via multimodal deep learning. Comput Struct Biotechnol J. 2021;20:333–42.
2. Oakman C, Pestrin M, Zafarana E, Cantisani E, Di Leo A. Role of lapatinib in the first-line treatment of patients with metastatic breast cancer. Cancer Manag Res. 2010;2:13–25.
3. Xin Y, Guo WW, Huang Q, Zhang P, Zhang L, Jiang G, et al. Effects of lapatinib or trastuzumab, alone and in combination, in human epidermal growth factor receptor 2-positive breast cancer: a meta-analysis of randomized controlled trials. Cancer Med. 2016;5:3454.
4. Hurvitz SA, Kakkar R. Role of lapatinib alone or in combination in the treatment of HER2-positive breast cancer. Breast Cancer. 2012;4:35–51.
5. Wahdan-Alaswad R, Liu B, Thor AD. Targeted lapatinib anti-HER2/ErbB2 therapy resistance in breast cancer: opportunities to overcome a difficult problem. Cancer Drug Resist. 2020;3:179–98.
6. Fearon AE, Carter EP, Clayton NS, Wilkes EH, Baker A, Kapitonova E, et al. PHLDA1 mediates drug resistance in receptor tyrosine kinase-driven cancer. Cell Rep. 2018;22:2469–81.
7. Jian W, Zhang X, Wang J, Liu Y, Hu C, Wang X, et al. Scinderin-knockdown inhibits proliferation and promotes apoptosis in human breast carcinoma cells. Oncol Lett. 2018;16:3207–14.
8. Garcia-Martinez L, Zhang Y, Nakata Y, Chan HL, Morey L. Epigenetic mechanisms in breast cancer therapy and resistance. Nat Commun. 2021;12:1786.
9. Wang Y, Li Z, Bai L, Zhang D, Zhang T, Ren F. Scinderin is a novel oncogene for its correlates with poor prognosis, immune infiltrates and matrix metalloproteinase-2/9 (MMP2/9) in glioma. Brain Sci. 2022;12:1415.
10. Schratter G, Scheruebel S, Langthaler S, Ester K, Pelzmann B, Ghaffari-Tabrizi-Wizsy N, et al. GIRK1 triggers multiple cancer-related pathways in the benign mammary epithelial cell line MCF10A. Sci Rep. 2019;9:19277.
11. Sehgal P, Chaturvedi P. Chromatin and cancer: implications of disrupted chromatin organization in tumorigenesis and its diversification. Cancers. 2023;15:466.
12. Doll S, Gnad F, Mann M. The case for proteomics and phospho-proteomics in personalized cancer medicine. Proteom Clin Appl. 2019;13:e1800113.
13. de Nicola F, Corleone G, Goeman F. Dissecting the epigenome driving drug resistance by ATAC-seq. Methods Mol Biol. 2022;2535:171–85.
14. Lin Q, Li J, Zhu D, Niu Z, Pan X, Xu P, et al. Aberrant scinderin expression correlates with liver metastasis and poor prognosis in colorectal cancer. Front Pharmacol. 2019;10:1183.
15. Li W, Huang L, Qi N, Zhang Q, Qin Z. Upregulation of CALD1 predicted a poor prognosis for platinum-treated ovarian cancer and revealed it as a potential therapeutic resistance target. BMC Genom. 2024;25:183.
16. Balcioglu O, Gates BL, Freeman DW, Hagos BM, Mehrabad EM, Ayala-Talavera D, et al. Mcam stabilizes a luminal progenitor-like breast cancer cell state via Ck2 control and Src/Akt/Stat3 attenuation. NPJ Breast Cancer. 2024;10:80.
17. Gorbacheva AM, Uvarova AN, Ustiugova AS, Bhattacharyya A, Korneev KV, Kuprash DV, et al. EGR1 and RXRA transcription factors link TGF-β pathway and CCL2 expression in triple negative breast cancer cells. Sci Rep. 2021;11:14120.
18. Hayat A, Carter EP, King HW, Ors A, Doe A, Teijeiro SA, et al. Low HER2 expression in normal breast epithelium enables dedifferentiation and malignant transformation via chromatin opening. Dis Model Mech. 2023;16:dmm049894 https://doi.org/10.1242/dmm.049894.
19. Hanna A, Nixon MJ, Estrada MV, Sanchez V, Sheng Q, Opalenik SR, et al. Combined Dusp4 and p53 loss with Dbf4 amplification drives tumorigenesis via cell cycle restriction and replication stress escape in breast cancer. Breast Cancer Res. 2022;24:51.

20. Yang Y, Zhang J, Yan Y, Cai H, Li M, Sun K, et al. Low expression of Rap1GAP is associated with epithelialmesenchymal transition (EMT) and poor prognosis in gastric cancer. Oncotarget. 2016;8:8057–68.
21. Hayes JD, Dinkova-Kostova AT, Tew KD. Oxidative stress in cancer. Cancer Cell. 2020;38:167.
22. Rashid NS, Boyd DC, Olex AL, Grible JM, Duong AK, Alzubi MA, et al. Transcriptomic changes underlying EGFR inhibitor resistance in human and mouse models of basal-like breast cancer. Sci Rep. 2022;12:21248.
23. Sheng N, Yan L, Wu K, You W, Gong J, Hu L, et al. TRIP13 promotes tumor growth and is associated with poor prognosis in colorectal cancer. Cell Death Dis. 2018;9:402.
24. Zhang X, Shi L, Sun H, Wang Z, Xu F, Wei J, et al. IGF2BP3 mediates the mRNA degradation of NF1 to promote triple-negative breast cancer progression via an m6A-dependent manner. Clin Transl Med. 2023;13:e1427.
25. Jiang L, Liu Y, Pan Y, Tan Z, Wang J, Zheng G, et al. Silencing of AJAP1 expression by promoter methylation activates the Wnt/β-catenin signaling pathway to promote tumor proliferation and metastasis in salivary adenoid cystic carcinoma. Gland Surg. 2023;12:834.
26. Kuhara K, Tokuda K, Kitagawa T, Baron B, Tokunaga M, Harada K, et al. CUB domain-containing protein 1 (CDCP1) is down-regulated by active hexose-correlated compound in human pancreatic cancer cells. Anticancer Res. 2018;38:6107.
27. Park Y, Jung SY, Jennings NB, Rodriguez-Aguayo C, Peng G, Lee S, et al. FOXM1 mediates Dox resistance in breast cancer by enhancing DNA repair. Carcinogenesis. 2012;33:1843.
28. Barkardottir RB, Johannsdottir HK, Johannesdottir G, Agnarsson BA, Eerola H, Arason A, et al. Deletions on chromosome 4 in sporadic and BRCA mutated tumors and association with pathological variables. Anticancer Res. 2004;24:2681–7.
29. Panigrahi A, O'malley BW. Mechanisms of enhancer action: the known and the unknown. Genome Biol. 2021;22:108.
30. Yang W, Wang X, Zheng W, Li K, Liu H, Sun Y. Genetic and epigenetic alterations are involved in the regulation of TPM1 in cholangiocarcinoma. Int J Oncol. 2016;50:340.
31. Mendonça V, Soares-Lima SC, Moreira MAM. Exploring cross-tissue DNA methylation patterns: blood–brain CpGs as potential neurodegenerative disease biomarkers. Commun Biol. 2024;7:904.
32. Paris J, Wilhelm C, Lebbé C, Elmallah M, Pamoukdjian F, Héraud A, et al. PROM2 overexpression induces metastatic potential through epithelial-to-mesenchymal transition and ferroptosis resistance in human cancers. Clin Transl Med. 2024;14:e1632.
33. Zhang W, Zhou Q, Wei Y, Da M, Zhang C, Zhong J, et al. The exosome-mediated PI3k/Akt/mTOR signaling pathway in cervical cancer. Int J Clin Exp Pathol. 2019;12:2474–84.
34. Suresh R, Diaz RJ. The remodelling of actin composition as a hallmark of cancer. Transl Oncol. 2021;14:101051.
35. Li X, Zhao L, Chen C, Nie J, Jiao B. Can EGFR be a therapeutic target in breast cancer? Biochim Biophys Acta Rev Cancer. 2022;1877:188789.
36. Gallon J, Loomis E, Curry E, Martin N, Brody L, Garner I, et al. Chromatin accessibility changes at intergenic regions are associated with ovarian cancer drug resistance. Clin Epigenetics. 2021;13:122–6.
37. Murad R, Avanes A, Ma X, Geng S, Mortazavi A, Momand J. Transcriptome and chromatin landscape changes associated with trastuzumab resistance in HER2+ breast cancer cells. Gene. 2021;799:145808.
38. Audet-Delage Y, St-Louis C, Minarrieta L, McGuirk S, Kurreal I, Annis MG, et al. Spatiotemporal modeling of chemoresistance evolution in breast tumors uncovers dependencies on SLC38A7 and SLC46A1. Cell Rep. 2023;42:113191.
39. Hua L, Song Y, Min J, Wang R, Li H, Zhu L, et al. AKR7A3 modulates the metastasis of pancreatic ductal adenocarcinoma through regulating PHGDH-suppressed autophagy. Cancer Sci. 2023;114:3101–13.
40. Wang L, Yang H, Abel EV, Ney GM, Palmbos PL, Bednar F, et al. ATDC induces an invasive switch in KRAS-induced pancreatic tumorigenesis. Genes Dev. 2015;29:171–83.
41. Cadigan KM, Waterman ML. TCF/LEFs and Wnt signaling in the nucleus. Cold Spring Harb Perspect Biol. 2012;4:a007906 https://doi.org/10.1101/cshperspect.a007906
42. Iwafuchi-Doi M. The mechanistic basis for chromatin regulation by pioneer transcription factors. Wiley Interdiscip Rev Syst Biol Med. 2018;11:e1427.
43. Petri BJ, Piell KM, South Whitt GC, Wilt AE, Poulton CC, Lehman NL, et al. HNRNPA2B1 regulates tamoxifen- and fulvestrant-sensitivity and hallmarks of endocrine resistance in breast cancer cells. Cancer Lett. 2021;518:152–68.
44. Reddi KK, Guruvaiah P, Edwards YJK, Gupta R. Changes in the transcriptome and chromatin landscape in BRAFi-resistant melanoma cells. Front Oncol. 2022;12:937831.
45. Gupta R, Bugide S, Wang B, Green MR, Johnson DB, Wajapeyee N. Loss of BOP1 confers resistance to BRAF kinase inhibitors in melanoma by activating MAP kinase pathway. Proc Natl Acad Sci USA. 2019;116:4583–91.
46. Hsu JL, Hung M. The role of HER2, EGFR, and other receptor tyrosine kinases in breast cancer. Cancer Metastasis Rev. 2017;35:575.
47. Kumar N, Cramer GM, Dahaj SAZ, Sundaram B, Celli JP, Kulkarni RV. Stochastic modeling of phenotypic switching and chemoresistance in cancer cell populations. Sci Rep. 2019;9:10845.
48. Furrer D, Dragic D, Chang S, Fournier F, Droit A, Jacob S, et al. Association between genome-wide epigenetic and genetic alterations in breast cancer tissue and response to HER2-targeted therapies in HER2-positive breast cancer patients: new findings and a systematic review. Cancer Drug Resist. 2022;5:995.
49. Neve RM, Chin K, Fridlyand J, Yeh J, Baehner FL, Fevr T, et al. A collection of breast cancer cell lines for the study of functionally distinct cancer subtypes. Cancer Cell. 2009;10:515.

ACKNOWLEDGEMENTS

We thank Dr Salvatore Federico Pedicona for critically reading the manuscript. We thank the City St George's, University of London's imaging research facility (IRF) for the shared microscopy services. The authors extend their appreciation to Taif University, Saudi Arabia, for supporting this work through project number (TU-DSPP-2025-23).

AUTHOR CONTRIBUTIONS

Conceptualisation: AH; methodology: AH, JS, VR; software: AH, JS, VR, NEA; validation: NA, NA, IA, AH, JS; formal analysis: AH, JS, NA, IA, VR, NEA; resources: AH, JS; data curation: JS, AH, VR, NA, NEA; writing—original draft: AH, JS; writing—review and editing: AH, JS; visualisation: AH, JS; supervision: AH; project administration: AH; funding acquisition: AH, NA.

FUNDING

The authors acknowledge financial support from City St George's, University of London. The authors acknowledge financial support for the Image Resource Facility (IRF) Research Excellence Fund and from Making a Difference Locally (MADL). This research was funded by financial support from Taif University, Saudi Arabia, project TU-DSPP-2025-23.

COMPETING INTERESTS

The authors declare no competing interests.

ETHICS APPROVAL AND CONSENT TO PARTICIPATE

This study did not require ethics approval as it did not involve human participants, animal subjects or other sensitive data, and no personal or identifiable information was collected or used. As such, ethics committee review and approval were not necessary in accordance with the institutional regulations.

ADDITIONAL INFORMATION

Supplementary information The online version contains supplementary material available at https://doi.org/10.1038/s41416-025-03174-3.

Correspondence and requests for materials should be addressed to A. Hayat.

Reprints and permission information is available at http://www.nature.com/reprints

Publisher's note Springer Nature remains neutral with regard to jurisdictional claims in published maps and institutional affiliations.